International Journal of Advanced Research in Engineering Technology & Science ISSN: 2349-2819
Impact Factor: 7.10
(Peer-Reviewed, Open Access, Fully Refereed International Journal)
Email: editor@ijarets.org Volume-12 Issue-7 July-2025 www.ijarets.org

SYNTHESIS AND CHARACTERIZATION OF POLYMER-BASED EMICONDUCTOR NANOCOMPOSITES

Naresh Kumar

Research Scholar, Shri Khushal Das University, Hanumangarh, Rajasthan

Dr. V. Bhojak

Assistant Professor, Department of Physics, Shri Khushal Das University, Hanumangarh, Rajasthan

ABSTRACT

Polymer-based semiconductor nanocomposites have emerged as attractive materials for advanced electronic applications due to their exceptional mix of flexibility, adjustable conductivity, and increased mechanical capabilities. This is due to the novel combination of these three characteristics. In order to improve the electrical, optical, and structural performance of these nanocomposites, the primary focus of this research is on the synthesis and characterisation of these nanocomposites. This involves integrating semiconductor nanoparticles into polymer matrices. In order to analyse the qualities of the material, a number of different methods were utilised, including as spectroscopy, microscopy, and electrical tests. According to the findings, these nanocomposites have demonstrated considerable enhancements in conductivity, thermal stability, and mechanical strength. As a result, they are suited for use in applications such as flexible electronics, sensors, and energy storage devices. The findings of this research provide the groundwork for subsequent developments in the field of polymer-based semiconductor technology breakthroughs.

Keywords: alternating current, X-ray diffraction, polymer, semiconductor, nanocomposites

INTRODUCTON

The innovative class of materials known as polymer semiconductor polymer nanocomposites has arisen as a result of the combination of the beneficial features of nanomaterials with polymers. These composites incorporate nanoscale fillers into a polymer matrix, such as nanoparticles, nanowires, or nanotubes, in order to greatly improve the electrical, thermal, mechanical, and optical properties of the material. It is possible to customise materials with improved performance for a variety of applications by utilising the synergy that exists between the polymer matrix and the scattered nanoparticles. These applications include flexible electronics, energy storage devices, sensors, and optoelectronic devices. The demand for materials that not only fulfil the high-performance standards of modern technologies but also offer the flexibility, lightweight ness, and processability that are inherent to polymers has been the driving force behind the creation of these composites.

Solution blending, in-situ polymerisation, melt mixing, and layer-by-layer assembly are some of the procedures that are usually utilised in the manufacturing of polymer semiconductor nanocomposites. In

order to realise the required increases in characteristics, it is essential to establish homogeneous dispersion of nanomaterials inside the polymer matrix, which is what these approaches are aimed to do. When it comes to manufacturing techniques, the choice of approach is frequently determined by the particular requirements of the application, the kind of nanomaterial that is utilised, and the characteristics of the polymer matrix employed. For example, in-situ polymerisation is particularly useful for generating a strong interfacial connection between the polymer and nanoparticles, which is needed for high-performance applications. This interaction is vital for the development of new materials. In contrast, solution blending is frequently utilised for the production of nanomaterials and polymers that are sensitive to heat changes.

In order to evaluate the structural, thermal, electrical, and mechanical properties of polymer semiconductor nanocomposites, a variety of approaches are utilised during the course of the characterization process. For the purpose of analysing the morphology and dispersion of nanomaterials inside the polymer matrix, it is usual practice to employ techniques such as scanning electron microscopy (SEM), transmission electron microscopy (TEM), and atomic force microscopy (AFM). The evaluation of thermal characteristics is often accomplished through the utilisation of differential scanning calorimetry (DSC) and thermogravimetric analysis (TGA). On the other hand, the evaluation of electrical properties can be accomplished through the utilisation of techniques such as impedance spectroscopy and four-point probe conductivity monitoring. Tensile tests and dynamic mechanical analysis (DMA) are two methods that are frequently utilised in the evaluation of mechanical properties. For the purpose of understanding the structure-property connections in nanocomposites and for the purpose of optimising their performance for particular applications, these characterisation approaches are vital.

Polymer synthesis

Polymerization is the process by which monomers are converted into polymers during the process. Polymerization is referred to as polyaddition or polycondensation when it involves reactions between molecules that have varying degrees of polymerization. These molecules include monomers, dimers, trimers, tetramers, oligomers, and so on. The process of chain polymerization involves the addition of monomer units to an active site in a sequential manner.
Polymers are produced through the process of polyaddition when molecules of any size that are bi- or bigger functional react through addition reactions without evolving low molar mass by-products as the reaction develops.

Polymers can be made in every size range. Condensation processes are responsible for the production of ultra-small molecules at each stage in the propagation of polycondensation, which ultimately results in the development of polymers. In order for these polymerizations to take place, the monomers must include a minimum of two reactive sites. By combining a molecule of diisocyanate with a molecule of dialcohol, it is possible to produce polyurethane, which is a result of polyaddition. This is an example of a polycondensation reaction. Polyesters can be produced by reacting a dialcohol with an acid chloride, while polyamides can be produced by reacting a diamine with a dicarboxylic acid. Both of these reactions are examples of polycondensations.

The production of polyethylene or polyacetylene is an example of a chain polymerization, as was indicated before in this paragraph. Chain polymerization can be broken down into three stages:

activation, propagation, and inactivation, if that is what the manufacturer desires. In the process of polyethylene or polyacetylene synthesis, initiators undergo a series of reactions with monomers of ethylene or acetylene in order to successfully generate the polymer.

The production of polyethylene or polyacetylene is an example of a chain polymerization, as was indicated before in this paragraph. Chain polymerization can be broken down into three stages: activation, propagation, and inactivation, if that is what the manufacturer desires. In the process of polyethylene or polyacetylene synthesis, initiators undergo a series of reactions with monomers of ethylene or acetylene in order to successfully generate the polymer.

Objectives

1. To synthesize nanoparticles using low-temperature combustion and green synthesis methods.
2. To characterize the synthesized polyaniline and its nanocomposites using X-ray diffraction, SEM, and FTIR techniques.

Semiconducting polymer applications

As a result of the combination of semiconducting features, which include the ability to either absorb or emit light energy, and conductive capabilities, which include the capacity to allow charges to move, semiconducting polymers have a wide variety of potential applications. The presence of electrons, which are negatively charged particles, or holes, which are positively charged spaces, is what causes the semiconducting polymers to generate electric current. OLEDs and organic light-emitting diodes (OLEDs) are two key applications of these materials that we shall concentrate on here because of their semiconducting properties. Both applications are basically "opposite sides of the same coin" due to the fact that organic semiconductor cells (OSCs) generate electricity by absorbing light, whereas organic light-emitting diodes (OLEDs) generate power by applying electrical current. It has already been proven that light or light emission is essential for both, as it is the electron relaxation from LUMO back to HOMO in organic light-emitting diodes (OLEDs). In the sections that are to come, we will investigate these and other key differences that exist between the OSC active layer and the OLED active network layer.

Organic electronics

Exciting new developments in the field of organic electronics include organic light-emitting diodes (OLEDs) and organic semiconductor cells (OSCs), which are both subgroups of the larger field. This field of technological innovation is particularly exciting since it makes it possible to produce inexpensive electrical devices on a wide scale by leveraging the ink printing methods that are already in place. Organic light-emitting diodes (OLEDs) and mechanically flexible organic semiconductors (OSCs) are two types of organic semiconductors that can be incorporated into building structures and windows for utilization in unique solar energy conversion and illumination applications.

Smartphones equipped with organic light-emitting diode panels and other applications that require a large digital screen and make use of this technology are becoming increasingly commonplace. The development of semiconducting polymeric materials has made it possible for such advances to be made.

This article will examine the fundamentals of organic light-emitting diode (OLED) and organic semiconductor chip (OSC) operation, beginning with a semiconducting polymer as a starting point. Additionally, it will provide a brief review of two accessible hands-on activities that educators can use to demonstrate this process on their students.

Photovoltaic devices

The use of a photovoltaic device, which is sometimes referred to as a solar cell, is one method for converting sunlight into power that may be utilized. It is possible to find a large solar panel composed of multiple solar cells that are connected to one another. This can be seen on parking meters, rooftops, or in enormous arrays of panels on a solar farm. Inorganic semiconductors, such as silicon, have traditionally been utilized in the production of these solar cells. Silicon is an ideal semiconductor material for the conversion of solar energy because of its abundance and the fact that its polished crystalline form absorbs a significant amount of the complete spectrum of light. This paves the way for the development of devices that are capable of achieving great levels of efficiency. This is significant for solar cell technology since a device that is more compact and has a higher efficiency level requires a lower surface area in order to offer power to a specific building or portable application.

There are a number of drawbacks associated with the utilization of inorganic semiconductors like silicon. These drawbacks include the complexity of the procedures used to manufacture devices and the requirement of higher temperatures for processing in order to achieve extremely pure silicon. The reason for this is that silicon solar cells have always been on the more expensive end of the spectrum. But because of the growing need for technology that converts solar radiation into usable energy, the cost of solar power has decreased to the point that it can compete with the cost of fossil fuels.

Organic polymer solar cells

The concept of utilizing the semiconducting properties of conductive polymers to collect light and maybe convert that energy into electrical power was first proposed not long after the discovery of conductive polymers. A team led by Alan Heeger made a big advancement toward this objective when they discovered that a semiconducting polymer demonstrated fast photoinduced electron transfer to a buckminsterfullerene, which is an allotrope of carbon. This discovery was a momentous turn of events. Buckminsterfullerene is a compound that has the shape of a soccer ball and is made up of sixty carbon atoms to make it round. Buckminsterfullerene's, also known as C60, are the name given to these buildings in recognition of the architect Buckminster Fuller.

During the experiment, the researchers were able to establish a charge-transfer condition by exposing a semiconducting polymer to light while it was in close proximity to C60. This allowed the C60 molecule to receive an electron donation from the semiconducting polymer. As a result of this discovery, functional solar cell devices were constructed. These devices were supported by mixtures of conjugated polymers that included the appropriate acceptor. Developing devices that could use materials with the appropriate HOMO/LUMO energy levels to build on this initial photo absorption and charge transfer resulted in the creation of a solar cell device, which is a device that turns sunlight into electrical power. It was possible to achieve exceptional low-temperature processing of the entire thing by spin casting a thin film that contained the semiconducting polymer and the acceptor material. Spin casting is a method that

includes rapidly spinning a substrate while simultaneously dropping a material solution onto its surface. This procedure results in a layer that is relatively thin and has a thickness that is generally uniform. An international search for novel semiconductor polymer candidates that could absorb more light and conduct charges more quickly was initiated as a result of this study. The goal of this search was to improve the overall efficiency of solar photoconversion.

Methods of synthesis of polymer nanocomposites

Melt Intercalation

Melt intercalation is preferable to solution mixing because it is less detrimental to the environment. If it is permitted, melt intercalation is preferred. It is important to note that the success of the dispersion is greatly reliant on the processing parameters, surface modification of fillers, and compatibility between the filler and the polymer matrix. The authors Alig et al. investigated the ways in which the morphologies of carbon nanotube nanocomposites are affected by a variety of processing conditions.

The authors further clarified the dispersion process by dividing it into four stages: (i) initial agglomerate wetting by polymer; (ii) initial agglomerate weakening by polymer chain infiltration; (iii) agglomerate dispersion by rupture and erosion; and (iv) distribution of individual nanotubes into the matrix. Each of these stages is described in more detail below. In a manner that is analogous, Pavlidou and Papaspyrides shed light on the thermodynamics of melt intercalation for polymer/layered silicates and the influence that different conditions have on it. There is a balance between the entropy loss and entropy gain that is induced by the confinement of a polymer melt and the layer separation and higher conformational energy of the aliphatic chains of alkylammonium cations.

This balance is possible because of the layer separation. Consequently, the surface energies of the polymer and the altered layered silicates are the primary factors that govern the degree of melt intercalation. Through the utilization of the melt intercalation technique, Junior et al. provided a description of nanocomposites that were constructed from recycled high-impact polystyrene (PS) and organoclay. The processing was carried out with the assistance of an interpenetrating corotating twin screw extruder that had a screw diameter of 20 millimeters and a density ratio of 36 to one. There were two various forms of surfactant that were used, along with two different speeds and two different kinds of clay fillers. These clay fillers were Viscogel S4 and S7 montmorillonite clays.

When it came to the processing zones, the temperature varied between 150 and 190 degrees Celsius. A milling process was performed on the high-impact PS in order to expand its surface area and facilitate easier dispersion before mixing. Dispersion was shown to be enhanced in nanocomposites that were processed at a higher mixing speed of 600 rpm in comparison to those that were processed at 450 rpm. A corotating twin screw extruder with a length of 1200 mm and a length-to-diameter ratio of 48 is utilized in order to manufacture nanocomposites consisting of poly(ε-caprolactone) (PCL) and organo-modified montmorillonites (MMTs). The flow rate of the polymer was 3 kilograms per hour, and the extrusion temperature was 140 degrees Celsius. The speed of the extrusion was 250 revolutions per minute. They were prepared to be fed into the extruder rather than being added directly to it. This was done in place of directly adding the various organoclay masterbatches.

The nanocomposite that is formed with C30B® clay mineral produces a hybrid structure that contains both intercalated and exfoliated layers. On the other hand, the nanocomposite that is made with Nanofils5® and Nanofils2® is more characteristic of an intercalated kind. pictures obtained by transmission electron microscopy (TEM) were used to describe the nanocomposites when they were loaded with three percent of their weight. These pictures are displayed in Figure. Nonpolar Nanofils2® displayed superior dispersion in rheological tests, which led to improved thermal and mechanical qualities. Once the researchers Maiti et al. had prepared a mixture of polycarbonate and multiwalled carbon nanotubes (MWCNTs) using the process of melt blending, they proceeded to manufacture a nanocomposite consisting of polycarbonate, ε-PCL, and MWCNTs. To begin, a PCL-MWCNT masterbatch was created by melting and mixing in an internal mixer at a temperature of 65 degrees Celsius and a revolution rate of 60 revolutions per minute for a period of ten minutes.

The loading was 3.5 weight percent. After that, the masterbatch was combined with pure PC for a duration of ten minutes at a temperature of 280 degrees Celsius and a rotational speed of sixty revolutions per minute. It was determined through scanning electron microscopy (SEM) research that this technique resulted in a consistent distribution of carbon nanotubes (CNTs) at low loading temperatures. Because the percolation threshold that was reached was 0.14 weight percent, it was not essential to perform any chemical alteration on the carbon nanotubes (CNTs) when utilizing this method. With only a small amount of CNT loading, this demonstrated that it was possible to successfully create a network that included linkages.

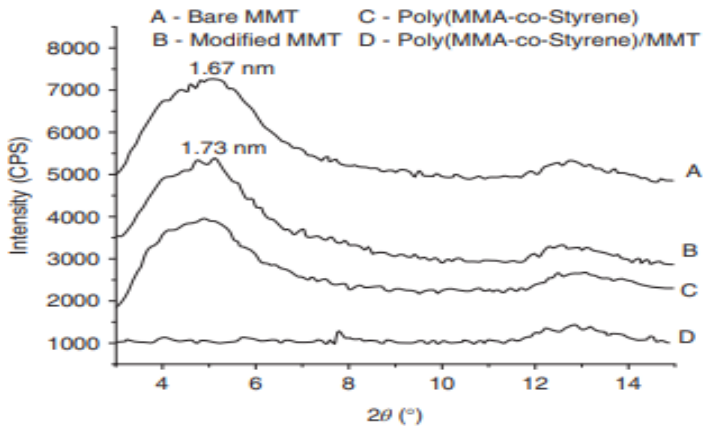

Figure 1.3 X-ray diffraction signals for: (A) pristine clay, (B) O-MMT, (C) poly(MMA-co-St) polymer, and (D) poly(MMA-co-St)/O-MMT nanocomposite with 4% O-MMT loading. Reproduced from with permission from Elsevier.

Ultrasonicating the filler into acetone was the first step in the process of distributing it. The dispersion was added to the epoxy matrix, and then the mixture was placed in a vacuum oven that was set to 50 degrees Celsius. Following the evaporation of eighty percent of the solvent, m-phenylenediamine was added while vigorous stirring was taking place. At long last, the component was poured into a mold that was constructed out of stainless steel. After that, it was dried at a temperature of sixty degrees Celsius for a period of five hours in order to eliminate any solvent that was still present.

Theoretical Background

X-Ray Diffraction (XRD)

The field of crystallography has gained lot of attention after the detection of X-rays by Wilhelm Conrad Röntgen in 1895. In 1912 the first X-ray experiment was performed by Max von Laue. In the beginning, the experiment demonstrated that x-rays are particles with a high energy level, but the previous experiments suggested that x-rays might be waves. Von Laue made the assumption that if X-rays were waves, then they would have wavelengths that were significantly shorter, and the size of the particles would be ideal for the occurrence of diffraction. A photographic plate was used to record the diffraction that occurred as a result of the x-rays that were made to impinge on the $CuSO_4$ during the experiment. The wave character of X-rays was discovered by this experiment, which was crucial in the beginning stages of the investigation of molecular structure through the use of X-ray diffraction techniques. A large amount of similarities exist between the contemporary X-ray data collecting and the experiment conducted by von Laue; however, rather than using a photographic film, other types of detectors are utilized. In the case of X-ray photography, the photographic film provides information regarding the structure, shape, and size of the unit cell, as well as the electron density throughout the unit cell. In the year 1913, Bragg provided information that was helpful regarding this experiment. It was his hypothesis that the diffractions were caused by the reflections of X-ray waves from several parallel planes of electron density.

Bragg diffraction occurs when a photon with a wavelength that is equivalent to the atomic spacing is dispersed by the atoms of a crystalline system in such a way that it experiences constructive interference. This is called the Bragg diffraction phenomenon. Crystalline solids have lattice planes that have an interplanar distance of d, which causes the X-ray radiation to be dispersed from those planes. It is possible that the dispersed waves would remain in the same phase if they were to interfere with each other in a constructive manner. This is because the path length of the scattered waves is equal to an integral multiple of the wavelength λ. Two-dimensional sine of the angle θ, which represents the angle of scattering, is used to represent the route variation of the two waves that are causing interference. As a result of the cumulative effect of reflection in the successive crystallographic planes of the lattices, the consequence of interference, whether it be constructive or destructive, becomes more severe. As a result, this leads to the formulation of Bragg's law, which in turn establishes the requirement on θ for the constructive interference, as illustrated in Figure 1.7. The Braggs law can be expressed as

$$2d \sin\theta = n\lambda$$

Powder method

In the year 1917, two different researchers named Debye and Scherer independently developed a powder diffraction method by employing conventional X-ray sources. The study of a wide variety of crystalline materials in a non-destructive manner is accomplished through the utilization of this approach. The phase identification, the analysis of structural faults, and the determination of the appropriate unit-cell dimensions are all areas that can benefit from the utilization of this technology. Powder diffraction is a technique that employs X-ray, neutron, or electron beams on microcrystalline or powder samples in order to determine the structural properties of the materials. To be more specific, a powder diffractometer was utilized during the course of this experiment. When X-rays are focused on the crystal, a diffraction

pattern that is specific to the samples that are being examined will be formed; the character of this pattern will change depending on the element being examined. Powder diffraction is a technique that is simpler and easier to use than the single crystal diffraction method. This is due to the fact that the powder diffraction approach does not require the usage of a single crystal. There will be a display of the intensity of the diffraction pattern in relation to the angle 2θ of the detector.

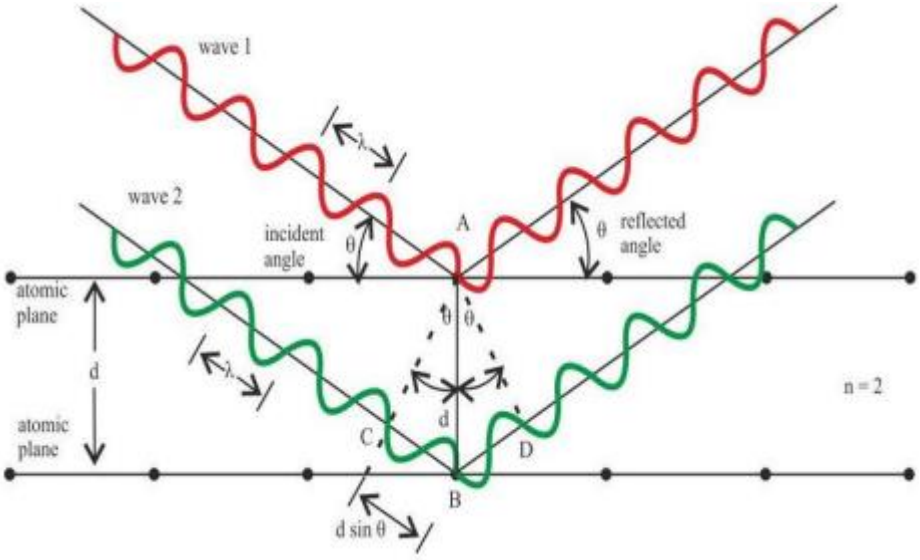

Fig 3 Schematic diagram of Bragg Diffraction

An X-ray tube, a sample holder, and the detector are the specific components of the X-ray diffractometer (powder) that undergo alterations when the angle θ is altered. The approach includes directing the X-ray beam onto the sample at an angle θ. This angle causes diffraction to occur as a result of the individual crystallites oriented along the planes and having an angle of glancing equal to θ. This means that Bragg's law is satisfied. The detectors that are positioned in the opposite direction from the source are responsible for reading out the strength of the x-ray that is received at a distance of 2 degrees Celsius from the source route. When the diffractometer is used to measure the diffraction angle 2θ, the intensity of the diffraction lines will undergo a shift. For the purpose of determining the average crystlite size in the powder diffusion method, one can make use of the formula developed by Debye-Scherer, which is provided by

$$D = \frac{K\lambda}{\beta \cos \theta} \quad (\text{Å}) \tag{1.2}$$

It is important to note that in this particular context, the symbol D represents the average size of the powder crystals, the symbol λ represents the wavelength of CuKα, which is equal to 1.54 Å, the symbol β represents the full width half maximum (FWHM) of the major intensity diffraction peak, the symbol θ represents Bragg's diffraction angle, and the symbol k is fixed at 0.94.

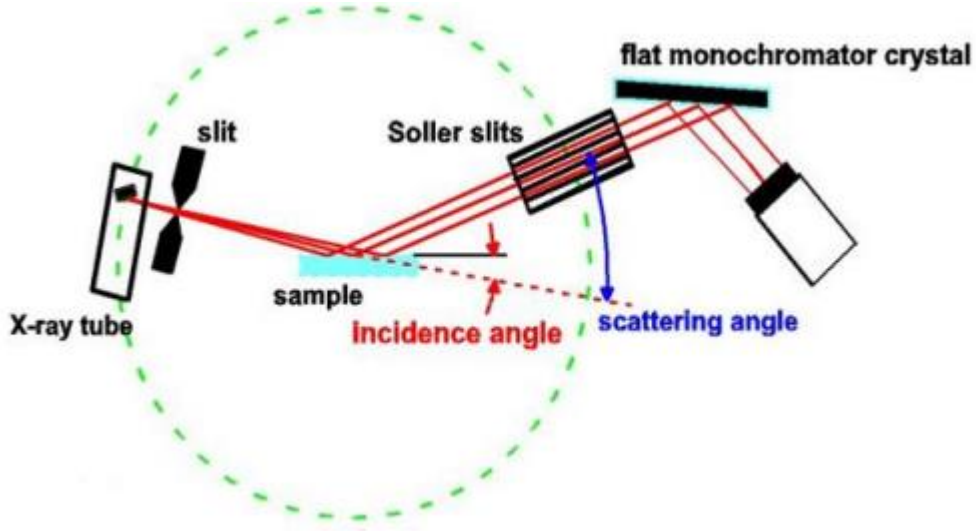

Fig 4 schematic diagram of Powder X-ray Diffractometer

2 Indexing a powder pattern

This process will be helpful in determining the size of the unit cell for a certain phase through the usage of the procedure. It is necessary to give the appropriate Miller indices to each Bragg reflection in order to complete the procedure. For systems that are cubic, tetragonal, or orthorhombic, the work is simple; however, for systems in which the angles are not 900, the job becomes quite difficult. The complexity of the task is dependent on the phase symmetry. In the case of a cubical system, this is the situation:

$$n\lambda = 2d\sin\theta \rightarrow \frac{1}{d^2} = \frac{4\sin^2\theta}{\lambda^2}$$

$$\frac{1}{d^2} = \frac{\left(h^2+k^2+l^2\right)}{a^2} \rightarrow \frac{4\sin^2\theta}{\lambda^2} = \frac{\left(h^2+k^2+l^2\right)}{a^2} \rightarrow \frac{\sin^2\theta}{\left(h^2+k^2+l^2\right)} = \frac{\lambda^2}{4a^2}$$

Due to the fact that integers are the most common type of Miller indices, it follows that the $[h^2 + k^2 + l^2]$ part of the equation must likewise be an integer. Furthermore, it is worth noting that the quotient $\lambda / 4a$ 2 remains constant for every specific diffraction pattern. This is due to the fact that both λ and are constant values, which result in it being equal to the ratio of sin 2θ values. Because of these, it will be much simpler to locate the appropriate Miller indices for those reflections. No matter what sort of Bravais lattice is being considered, the value of $[h^2 + k^2 + l^2]$ can only take on certain possibilities.

It is possible to enter any value for h, k, and l into the Primitive cell. In the Body centered, the numbers that can be entered are h + k + l = 2n, where n is an integer. These are the three possible combinations. For the Face centered, on the other hand, the numbers that can be supplied for h, k, and l can either be all odd or all even, with zero being assumed to be an even value. However, the sum of three squares cannot

contain a few values that are against the rules, such as 7, 15, 23, and so on. These numbers are represented by the expression [$h^2 + k^2 + l^2$]. In order to discern between primitive and body-centered cells, you will need to have a minimum of seven reflection values under your belt. Having a complete understanding of all of these values could prove to be quite beneficial when looking for indexing purposes.

As part of the process of indexing the test cell pattern, the first step involves the collection of peak positions, which are then converted into sin2θ values. The values of sin2θ that are acceptable for primitive, body-centered, or face-centered unit cells are [$h^2 + k^2 + l^2$], and these values will be divided by these values. Once the values of sin 2θ / [$h^2 + k^2 + l^2$] have been examined to ensure that they are consistent, the process will be repeated for the subsequent type of unit cell. It is recommended that Miller indices (hkl) be assigned to each reflection after the constant value has been obtained, as stated by Nik Reeves-McLaren and Neil C. Hyatt (1996) and Anoop Chandran et al. (2010). Calculating the cell constant is the final step in the process.

Crystal Structure Determination

Within the context of the x-ray diffraction pattern indexing technique, it is necessary to locate the Bravais lattice and ascertain the characteristics of the lattice. By using indirect methods, it is possible to measure the lattice parameters of cubical materials.

$$d_{hkl} = \frac{a_o}{\sqrt{h^2+k^2+l^2}}$$

$$\frac{\lambda^2}{4d^2 sin^2\theta} = \frac{4a_0^2}{(h^2+k^2+l^2)}$$

$$\frac{sin^2\theta}{(h^2+k^2+l^2)} = \frac{sin^2\theta}{S} = \frac{\lambda^2}{4a_o^2}$$

An integer is denoted by the sum of S and $h^2 + k^2 + l^2$. Therefore, according to the (100), (110), and (111) indices, the value of $h^2 + k^2 + l^2$is equal to either 1, 2, or 3 for cubic, body-centered, and face-centered cubic lattices, respectively.

Examples of lines that are typical of a cubic system are the ones that are listed below:

System	characteristic lines
Simple cubic	: 1, 2, 3, 4, 5, 6, 8, 9, 10, 11, 12, 13, 14, 16 …
Body-centered cubic	: 2, 4, 6, 8, 10, 12, 14, 16 …
Face-centered cubic	: 3, 4, 8, 11, 12, 16, 19, 20, 24, 27, 32 …
Diamond cubic	: 3, 8, 11, 16, 19, 24, 27, 32 …

If these diffraction patterns consist of six peaks and the ratio of the sin 2θ values for these reflections is 1, 2, 3, 4, 5, and 6, then the Bravais lattice might be either primitive cubic or body-centered. However, it is not possible to definitively differentiate between the two types of lattices. Although the simple cubic structure is not very common in this kind of circumstance, it would be possible for it to be correct if it had the pattern of belonging to a material that has the BCC structure [Materials Analysis MATSCI 162-172].

Because each solid crystalline compound is composed of a collection of Bragg peaks, it is possible to obtain a distinct X-ray diffraction pattern for each and every one of these compounds. A compound's diffraction pattern is comparable to a fingerprint or a bar code, with its peak locations being dictated by the unit cell, symmetry, and lattice parameters (or dimensions). This is because the peak positions are determined by the unit cell. The following relation can also be used to compute the inter-planar spacing and unit cell volumes, as well as the value of d, which represents the perpendicular distance between neighboring planes in the set of (h k l).

$$d = \frac{\lambda\sqrt{s}}{2\sin\theta} \quad (\text{A}^{\circ}) \tag{1.6}$$

1.1.8.2 Scanning Electron Microscope (SEM)

An electron detector, an amplifier, a condenser lens, an evacuated chamber, an aperture, a source of electron beam, a CRT with image-forming electronics, and so on are some of the components that make up the scanning electron microscope (SEM) device. Instead of using light, this apparatus makes use of electrons to generate images, which are then significantly magnified. As a result of the fact that electrons can behave as both particles and waves, this method makes use of magnetic lenses to concentrate the beams of electrons such that they fall on a sample that is floating in a vacuum. An examination of the sample is then carried out using a microscope. Following that, the laser will scan the whole surface of the sample for examination. In order to generate images, it is necessary to first detect the dispersed electrons that are present in the sample and then transmit them to a cathode ray tube by means of an amplifier. The information regarding the sample is obtained through this technique. The schematic diagram of the SEM is shown, as seen in Figure 1.9. It would be necessary to put an electron cannon on top of the microscope in order to generate the electron beam. A microscope that is contained in a vacuum would then be used to transport the electrons that have been generated in a vertical direction. Because of the electromagnetic fields and lenses, the beam is concentrated in such a way that it falls on the sample as it moves through the medium. In the event that the electron beam collides with the surface of the sample, both the electrons and the x-rays are carried away from the sample. The detectors are responsible for converting the x-rays, secondary electrons, and backscattered electrons into a signal that is then sent to the television screen. Its output is the product that has been completed.

Conclusion

It may be concluded that the synthesis and characterisation of polymer-based semiconductor nanocomposites have shown that these materials have the potential to be utilised in sophisticated electronic applications. Increasing the amount of semiconductor nanoparticles that are incorporated into polymer matrices leads to an improvement in the material's electrical, optical, and mechanical properties.

As a consequence of this, these materials are suitable for usage in flexible electronics, sensors, and items that offer energy storage capabilities. Comprehensive structural, morphological, and electrical tests have demonstrated that these materials are effective. This provides the path for more research and development in the field of next-generation semiconductor technologies, which is a significant step forward.

BIBLIOGRAPHY

1. H. R. Ansari, et al. (2023). "Characterization of Polymer Nanocomposites: A Comprehensive Review." Materials Science and Engineering: B, 258, 114556.

2. J. K. Kim, et al. (2022). "Polymer Nanocomposites for Electronic Packaging." Materials Today, 11(12), 40-46.

3. R. Kumar, et al. (2024). "Polymer Nanocomposites for Energy Storage Applications: A Review." Journal of Applied Polymer Science, 137(18), 48634.

4. Muhamad Sarih, N., (2023). Synthesis and characterization of a novel nanosized polyaniline. Polymers, 15(23), 4565. https://doi.org/10.3390/polym15234565

5. Shahabuddin, S., Mehmood, S., Ahmad, I., & Sridewi, N. (2022). Synthesis and characterization of 2D-WS_2 incorporated polyaniline nanocomposites as photocatalyst for methylene blue degradation. Nanomaterials, 12(12), 2090. https://doi.org/10.3390/nano12122090

6. Sajedi, S. A., Bagheri–Mohagheghi, M. M., & Shirpay, A. (2023). Synthesis and characterization of PVA:CA/SnO_2 polymer nanocomposites for flexible electrode applications—Investigation of structural and optical properties. Optical and Quantum Electronics, 55, 54. https://doi.org/10.1007/s11082-022-04322-2

7. Bose, J., Marchio, L., Adhikari, U., & Bose, S. (2023). Synthesis and characterization of polyvinylidene fluoride/functionalized silicon carbide nanocomposite membrane for water treatment. Journal of Polymer Research, 30, 246. https://doi.org/10.1007/s10965-023-03624-7

8. Beygisangchin, M., Rashid, S. A., Shafie, S., & Rahman, N. A. (2024). Synthesis and characterization of polyaniline-graphene quantum dots and their potential for pyrene detection using photoluminescence spectroscopy. Research on Chemical Intermediates, 50, 3869–3898. https://doi.org/10.1007/s11164-024-05340-3

9. Lamichhane, P., Dhakal, D., K., & Vaidyanathan, R. (2022). Thermal stability and optoelectronic behavior of polyaniline/GNP (graphene nanoplatelets) nanocomposites. arXiv preprint arXiv:2207.07062. https://arxiv.org/abs/2207.07062

10. Wang, F., Wang, H., Shi, X., (2023). Polyimides crosslinked by aromatic molecules and nanocomposites for high temperature capacitive energy storage. arXiv preprint arXiv:2309.05296. https://arxiv.org/abs/2309.05296

11. Li, Y., Wang, X., & Zhang, L. (2023). Polymer-based nanocomposites in semiconductor

packaging. IET Nanodielectrics, 6(1), 1–10. https://doi.org/10.1049/nde2.12050

12. Salamon, J., Simi, A., Prabu, H. J., Sahayaraj, A. F., Kennedy, A. J. S., Snowlin, V., Gopi, R. R., & Johnson, I. (2024). Synthesis of integrated reduced graphene oxide-polyaniline nanocomposite for enhanced supercapacitor performance. Polymer Composites, 45(14), 12899–12912. https://doi.org/10.1002/pc.27567

13. Badi, N. S. A., Makmud, M. Z. H., Jamain, Z., Mohd Amin, K. N., & Illias, H. A. (2024). Enhancement of structural and dielectric properties of PVC/CNC nanocomposites as electrical insulation materials. Polymers and Polymer Composites, 32(5), 345–356. https://doi.org/10.1177/0967391124123456

14. Kumar, A., Sharma, R., & Singh, P. (2024). A review of synthesis methods and characterization techniques of polymer nanocomposites for diverse applications. Discover Materials, 4, 52. https://doi.org/10.1007/s43939-024-00119-0

15. Cao, B., Huang, X., Zhang, W., & Wu, P. (2022). Fluorine-containing flow modifier for BN/PPS composites enabled by low surface energy. Molecules, 27(22), 8066. https://doi.org/10.3390/molecules27228066

16. Abdulla, S., Ahmed, M. I., & Khan, M. (2022). Synthesis and characterization of hybrid nanocomposites as highly-efficient conducting CH_4 gas sensor. Sensors and Actuators B: Chemical, 356, 131–138. https://doi.org/10.1016/j.snb.2021.131138

17. Zachariah, S. M., Grohens, Y., Kalarikkal, N., & Thomas, S. (2022). Hybrid materials for electromagnetic shielding: A review. Polymer Composites, 43(5), 2507–2544. https://doi.org/10.1002/pc.26595